Ferroelectric polarization-leakage current relation in high quality epitaxial $Pb(Zr,Ti)O_3$ films

L. Pintilie
NIMP, P.O. Box MG-7, 077125 Bucharest-Magurele, Romania and Max Planck Institute of Microstructure Physics, Weinberg 2, 06120 Halle, Germany

I. Vrejoiu, D. Hesse, G. LeRhun, and M. Alexe
Max Planck Institute of Microstructure Physics, Weinberg 2, 06120 Halle, Germany
(Received 7 September 2006; revised manuscript received 2 November 2006; published 8 March 2007)

Leakage current measurements were performed on epitaxial, single-crystal quality $Pb(Zr,Ti)O_3$ films with thicknesses in the 50–300 nm range. It was found that the voltage behavior of the leakage current has a minor dependence on thickness, which rules out the space-charge limited currents as main leakage source. Temperature-dependent measurements were performed to obtain more information on the transport mechanism through the metal-ferroelectric-metal (MFM) structure. The results are analyzed in the frame of interface-controlled Schottky emission. A surprisingly low value of only 0.12–0.13 eV was obtained for the potential barrier, which is much smaller than the reported value of 0.87 eV [I. Stolichnov *et al.*, Appl. Phys. Lett. **75**, 1790 (1999)]. The result is explained by the effect of the ferroelectric polarization on the potential barrier height. The low value of the effective Richardson constant, of the order of 10^{-7}–10^{-6} $A/cm^2\,K^2$, suggests that the pure thermionic emission is not the adequate conduction mechanism for epitaxial MFM structures. The true mechanism might be interface-controlled injection, followed by a low mobility drift through the film volume.

DOI: 10.1103/PhysRevB.75.104103 PACS number(s): 77.80.−e, 73.40.Sx, 77.84.Dy

I. INTRODUCTION

The origin of the leakage current in metal-ferroelectric-metal (MFM) structures based on lead zirconate titanate (PZT) materials is still subject to debate.[1] Many models were proposed to explain the voltage dependence of the leakage current in MFM structures, but most of these models are based on measurements performed on polycrystalline or defective layers.[2–11] The presence of intergrain boundaries, different types of dislocations (misfit, threading, etc.), and domain walls was neglected despite the fact that these extended structural defects can act as trapping and scattering centers for the injected mobile carriers leading to considerable reduction of carrier density and mobility. Such extrinsic effects can make a MFM structure look more resistive than the PZT material is itself.

The electrode-ferroelectric interface also plays an important role in the magnitude and voltage dependences of the leakage current. The most common studied MFM structures based on PZT employ Pt or $SrRuO_3$ (SRO) electrodes. It is generally accepted that both types of electrodes form Schottky contacts with PZT; thus, the possible presence of depletion layers near the contacts in MFM structures cannot be neglected.[12–14] Such high-resistance layers can induce an "insulating" appearance even if the material itself has pronounced semiconductor properties.

The effect of the microstructure onto the macroscopic electric properties might be considerable, and thus the development of theoretical models without considering these effects is not appropriate. The charge transport properties can be completely different in a single crystal and in a ceramic-like film. However, in order to study the intrinsic transport properties, the experimental measurements should be performed on high quality, single-crystal samples. This was the procedure in the case of standard semiconductors, such as Si or GaAs, and the same path should be followed in the case of ferroelectric PZT. Unfortunately, it is not possible to grow large single crystals of PZT due to the incongruent melting of the solid solution.[15,16] One way to obtain single-crystal-like samples is to grow high quality epitaxial films. Even in this case, the PZT layer can contain a considerable amount of extended defects such as dislocations and domain walls, as well as point defects such as vacancies and impurities.[17–20] If we want to have some indications of what might be the intrinsic conduction mechanisms in PZT, then we have to make considerable efforts to grow films with reduced defect densities, preferably defect-free.

In this paper, we report on leakage current measurements performed on epitaxial PZT films with different thicknesses. The experimental results suggest that the charge transport mechanism through single-crystal PZT is interface controlled. Then, the temperature dependence of the current-voltage (*I-V*) characteristic was studied and analyzed in the frame of the Schottky emission. The emerging values for the potential barrier and the Richardson constant are much lower than expected. The results are discussed by considering the probable effect of ferroelectric polarization on the barrier height and by assuming that the carrier injection is interface limited, but the charge transport through the film volume might be bulk limited.

II. EXPERIMENTS ON PZT

A. Growth and characterization methods

PZT films with a Zr/Ti ratio of 20/80 were grown by pulsed laser deposition (PLD) onto vicinal $SrTiO_3$ (001) substrates. A 20-nm-thick $SrRuO_3$ (SRO) film was deposited first as a bottom electrode. The PZT20/80-SRO pair was not randomly selected, because it has a very good lattice match, reducing the probability of misfit dislocations and increasing

 ©2007 The American Physical Society

the possibility to obtain high quality, epitaxial structures. The thickness of the PZT films was varied between 50 and 300 nm.

The quality of the epitaxial PZT films was investigated by various methods, such as transmission electron microscopy (TEM), atomic force microscopy, and piezoresponse force microscopy (PFM). Details about the growth mechanism and the structural characterization can be found elsewhere.[19,20] It was found that the amount of the extended structural defects is very much reduced in the studied films. Both the TEM and PFM investigations have shown that some 90° domains occur only above about 120 nm film thickness, but still their density is very low up to more than 270 nm thickness. In fact, below 120 nm, the films can be considered free of extended defects, as no dislocations or domain walls were observed in the TEM photographs. Extended defects might build up in films thicker than 120 nm, but in any case, the density is orders of magnitude lower than in the samples used in a previous study.[21]

For electric measurements, top SRO electrodes of about 0.09 mm^2 area were deposited by room-temperature PLD through a shadow mask. Hysteresis measurements were performed in the dynamic mode using a TF2000 analyzer. The values of the equivalent dielectric constants were obtained from capacitance measurements performed with a HP4194A impedance and/or gain analyzer at zero voltage and with 100 mV amplitude of the ac probing signal. Current-voltage (*I-V*) characteristics were measured using a Keithley 6517 electrometer. The measurements were always performed only after saturating the polarization by applying a dc field with the same polarity as the voltage used for the *I-V* characteristic. The contribution due to polarization switching was minimized in this way. The *I-V* measurements at different temperatures were performed in a cryostat with liquid-He flow. This allows measurement in a temperature range between 4.2 and 400 K. The procedure was to stabilize the temperature at the second decimal and then measure the *I-V* characteristic after choosing the right delay time in order to measure a quasistatic dc current. Hysteresis measurements were also performed at some temperatures to monitor the existence of the current peaks confirming the presence of polarization switching.

B. Experimental results

1. Hysteresis loop and dielectric constant

Typical hysteresis loops are presented in Figs. 1(a) and 1(b) for the 50- and 270-nm-thick films, respectively. Several facts can be noted from the hysteresis measurements.

(1) The large value of the ferroelectric polarization. The obtained numbers, after correcting for leakage current contribution, are all around 100 $\mu C/cm^2$ regardless of the thickness of the film. These values are well above the theoretical predictions based on thermodynamic models[22] but are close to those predicted by newer theories on ferroelectricity,[23–25] based on the Berry phase concept. Values close to 100 $\mu C/cm^2$ were also reported by other groups.[26–28]

(2) The square shape of the loops, with a flat polarization value after switching. Practically, the saturation and remnant polarizations are the same.

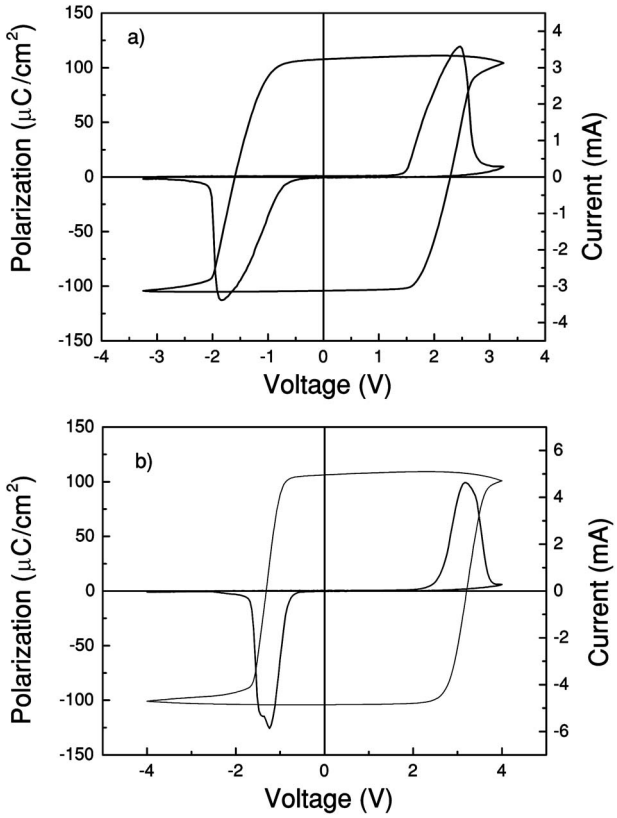

FIG. 1. Hysteresis loops (a) for a film with a thickness of 50 nm and (b) for a film with a thickness of 270 nm.

(3) The large values of the current peaks associated with the polarization switching. Although leakage is important, the switching peaks are at least one order of magnitude larger; therefore, it is not a problem to obtain good hysteresis loops.

The thickness dependence of the dielectric constant is shown in Fig. 2. As expected, the dielectric constant decreases with thickness. However, whereas the saturation toward large thickness confirms other reports,[29–31] the asymptotic behavior at lower thickness is an un-expected result. The dielectric constant saturates to around 280 for thick films, while for thinner films, it converges to about 80. The latter value is very close to the theoretical value of 86 calculated by Haun *et al.* along the *c* axis of the same PZT composition,[22] but it is almost twice the theoretical value calculated using quantum models.[25] The problem of the thickness dependence of the dielectric constant will be the subject of a separate study. However, this thickness variation raises a serious question regarding the value that should be used as material characteristic in the models developed to describe the electric properties of MFM structures. That is because the dielectric constant extracted from the measured capacitance, as for a plane-parallel capacitor, is a kind of global value of the structure, including a number of extrinsic effects coming from interfaces, charged defects, and domain walls (when the 90° domains are present). On the other hand,

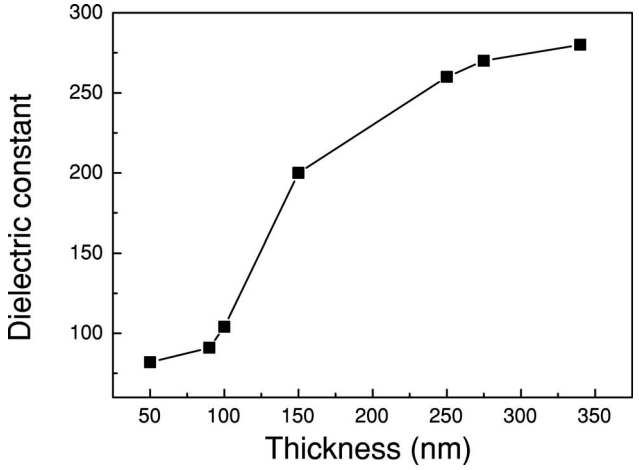

FIG. 2. Thickness dependence of the dielectric constant, as calculated from the measured capacitance and using the plane-parallel capacitor formula.

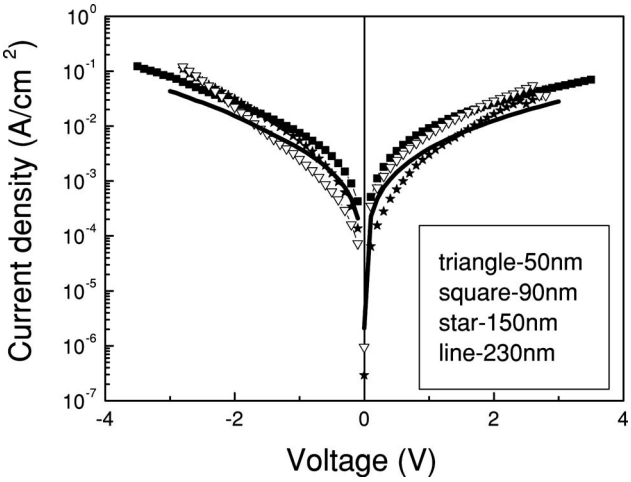

FIG. 3. *I-V* characteristics for PZT films with different thicknesses.

the value that should be used in equations is the intrinsic dielectric constant of the material, as is the case for Si or SiO_2. As mentioned above, the theoretically calculated values for dielectric constant or the values obtained from simulating capacitance-frequency dependency[25,32] are in the 30–40 range. However, the calculations and simulations are considering ideal structures with perfect lattice. The real structures are full of defects, distorting the lattice and adding extrinsic contributions to the dielectric constant. These contributions can be significantly higher in PZT compared with normal semiconductors such as Si, considering a larger polarizability of the ferroelectric and the higher amount of point defects (e.g., oxygen vacancies), which can reach 10^{20} cm^{-3}. The dielectric constant is important in calculating the electric fields, which, in turn, are important in estimating the current densities. The magnitude of the current flowing through a ferroelectric structure will be sensitive to the dielectric constant of the true structure. Furthermore, despite our belief that the intrinsic dielectric constant of PZT20/80 is around 30, we will consider that the value of 80 is the suitable dielectric constant for simulations performed on real structures. This value was experimentally obtained for thicknesses below 120 nm, where the extrinsic contributions to the dielectric constant arising from the 90° domains, domain walls, and dislocations are absent or diminished. At very small thicknesses, the PZT films are most probably fully depleted; thus, the extrinsic contribution due to the presence of Schottky interface capacitances is suppressed, the only extrinsic contribution that might still be present originating from point defects. The presence of a large amount of point defects makes the difference between the ideal lattice used for calculation of intrinsic dielectric constant and the real structure used for experiments. If the density of the point defects can be minimized, then the experimental value of the dielectric constant will approach the theoretical predictions.

2. Thickness and temperature dependences of the I-V characteristic

The experimental *I-V* characteristics for the films with thicknesses in the 50–300 range are presented in Fig. 3. Several observations can be made regarding these results.

(1) The current density values do not depend very much on thickness. The differences are below 1 order of magnitude for the used voltage range. This result excludes space-charge limited current (SCLC) as possible conduction mechanism in our PZT films. The SCLC has a thickness dependence as d^{-3}; thus, for a variation in film thickness d by about 6, the current magnitude should vary by at least 2 orders of magnitude.[33]

(2) Although the *I-V* characteristics show similar shapes, the positive and negative branches are not identical. In principle, bulk-controlled mechanisms should be symmetric to the change of the voltage polarity.[1] This is not the case. It might be argued that the asymmetry in the *I-V* characteristic might be induced by the imprint observed in the hysteresis loops. We did not notice any direct relation between imprint and *I-V* asymmetry. Capacitors with significant imprint can show a lower asymmetry than others with small imprint. The observed asymmetry suggests that the Poole-Frenkel (PF) emission from the traps is not an option in this case. The PF model was developed for a system of neutral atoms with no free electrons[34] and this might not be the case for the epitaxial PZT, which appears to have a free-carrier density far from being negligible. Another problem is that the PF model requires Ohmic-like contacts on the insulator, a situation which does not apply to the SRO-PZT system.

The above observations hint toward an interface-controlled mechanism, such as Schottky emission (SE) or Fowler-Nordheim tunneling (FN).[35,36] More information about the charge transport mechanism through the MFM structure can be obtained from temperature-dependent measurements. As it is known, the FN tunneling is virtually temperature independent, while the SE should present a strong temperature dependence. Therefore, one of the best samples (thickness of 215 nm) in terms of structure and polarization hysteresis was introduced into a cryostat for temperature measurements.

The experimental *I-V* characteristics at temperature steps of 10 K are shown in Fig. 4 for the 10–380 K temperature range.There are four distinctive region.

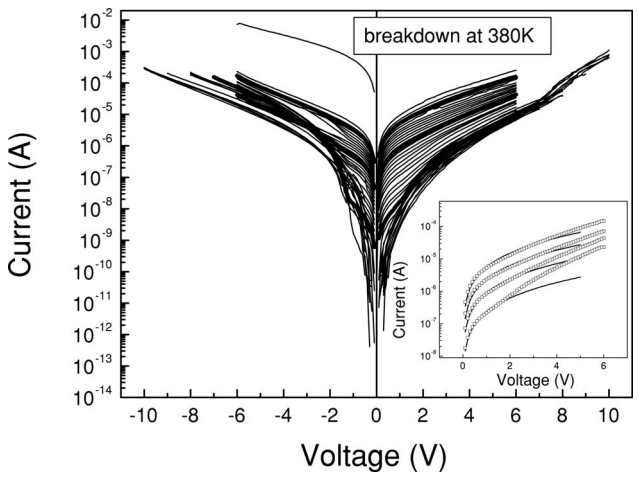

FIG. 4. *I-V* characteristics at different temperatures for a PZT film with a thickness of 215 nm. The thick lines limit the temperature domains with distinct conduction mechanisms: FN below 130 K, a mixture of FN and SE between 130 and 250 K, SE between 250 K and 350 K, and breakdown above 360 K. The inset shows the simulated *I-V* characteristics for temperatures of 200, 250, 300, and 350 K, together with the corresponding experimental curves. The simulations were performed using Eq. (14).

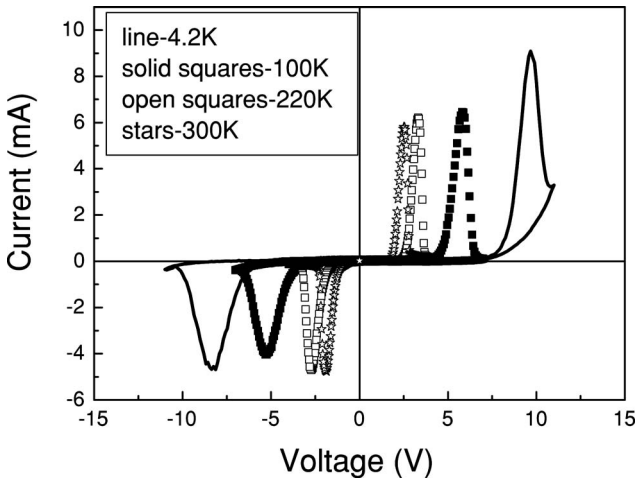

FIG. 5. Current hysteresis recorded during the polarization hysteresis measurement at different temperatures. The frequency of the triangular voltage was 1 kHz.

(1) Up to about 130 K, the *I-V* characteristics seem to be almost temperature independent, suggesting the dominance of the FN tunneling.

(2) Between 130 K and about 250 K, the charge transport seems to be a mixture of SE and FN, with SE dominant at low voltages and FN dominant at high voltages.

(3) Between 250 K and about 350 K, it appears that SE is the dominant mechanism, as the temperature dependence is very clear for most of the voltage range for both polarities.

(4) Above 360 K, some irreversible breakdown occurs, and at 380 K, the contact is totally damaged.

Regarding the hysteresis loop, the film is ferroelectric from the lowest temperature of 4.2 K up to the breakdown, as can be seen from Fig. 5 showing the current switching peaks.

The asymmetry of the two interfaces is even more visible in the temperature measurements presented in Fig. 4. We assume that the positive branch is for the bottom interface, which in TEM appears to be free from extended structural defects. This interface was processed at high temperature; thus, the structure is coherent and the layers are epitaxially grown. The top interface was processed at room temperature; therefore, it is expected to have a larger density of defects, especially dangling bonds forming interface states. Therefore, the electronic behavior will be different. In the following, the positive branch will be analyzed in more detail in order to extract some information on the interface properties.

Before the analysis, it is worth noting that the MFM structure can be regarded as a back-to-back connection of two Schottky diodes, assuming the presence of Schottky potential barriers at each SRO/PZT interface.[11] No matter what the polarity of the applied voltage on the top electrode, one of the diodes will always be reverse biased and the other forward biased. The current flowing through the MFM structure will be controlled by the reverse-biased contact.

First, we will focus on the SE mechanism, as from the Schottky representation it is possible to extract the potential barrier at the SRO/PZT interface. The Schottky equation for the current density in the case of thermionic emission is[33]

$$J = A^* T^2 \exp\left(-\frac{q}{kT}\left(\Phi_B^0 - \sqrt{\frac{qE_m}{4\pi\varepsilon_0\varepsilon_{op}}}\right)\right), \tag{1}$$

where A^* is Richardson's constant, Φ_B^0 is the potential barrier height at zero applied field, E_m is the electric field, T is the temperature, and ε_{op} is the dynamic (high-frequency) dielectric constant. The electric field E_m should be the maximum field at the Schottky interface.[33] This aspect will be discussed later in more detail. For the moment, we will consider the standard Schottky representation for a constant voltage, disregarding the voltage dependence of E_m. This representation is

$$\ln\left(\frac{J}{T^2}\right) = \ln(A^*) - \frac{q}{kT}\Phi_{app}, \tag{2}$$

where Φ_{app} is

$$\Phi_{app} = \Phi_B^0 - \sqrt{\frac{qE_m}{4\pi\varepsilon_0\varepsilon_{op}}}. \tag{3}$$

This is the apparent potential barrier, taking into consideration the barrier reduction due to the Schottky effect. Thus, the graphical representation $\ln(J/T^2)$-$1/T$ should be a straight line, and from its slope, it is possible to estimate the apparent potential barrier. Figure 6 shows these graphical representations for several voltages. Indeed, straight lines are obtained, but the temperature range diminishes as the voltage increases, probably due to a larger contribution from the FN tunneling.

Additionally, it will be assumed that the apparent barrier has a $V^{1/2}$ dependence. The Φ_{app}-$V^{1/2}$ representation should be a straight line, and the intercept should give the value of

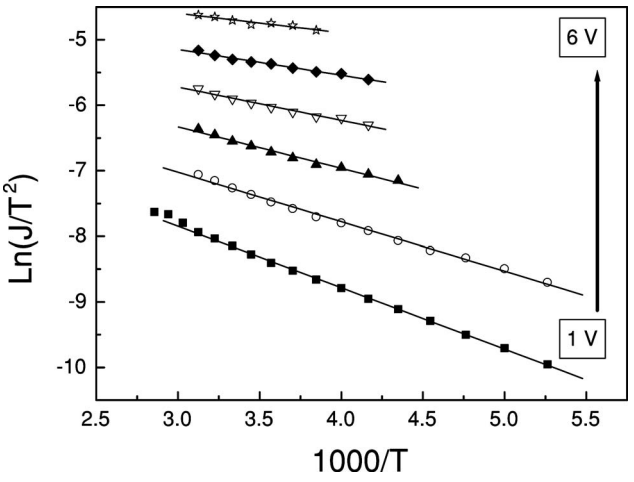

FIG. 6. Schottky representation (2) for different positive voltages.

Φ_B^0. The graph is shown in Fig. 7. The linear fitting is very good, confirming the $V^{1/2}$ dependence, but the intercept value gives a potential barrier at zero voltage of only 0.123 eV. This value is much smaller than the previous value of 0.87 eV reported by Stolichnov *et al.* in Ref. 11. Returning to the representation (2), the effective Richardson constant A^* can be evaluated from the intercept. The problem is that the obtained values are very small and seem to be voltage dependent, as shown in Fig. 8. This result suggests that Eq. (1) for the current density might not be appropriate.

It is possible to use an alternative form of the Schottky representation as follows

$$\ln\left(\frac{J}{T^2}\right) \sim \left(\ln(A^*) - \frac{q\Phi_B^0}{kT}\right) - f(V^{1/2}). \tag{4}$$

The first term in the right side is, in principle, voltage independent,

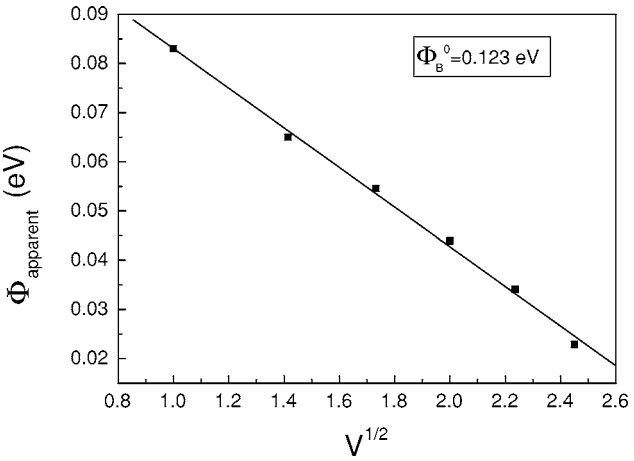

FIG. 7. Voltage dependence of the apparent potential barrier. The intercept gives the potential barrier at 0 V, which is about 123 meV.

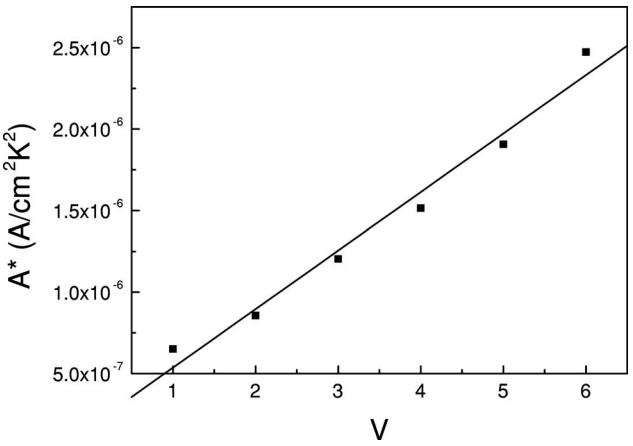

FIG. 8. The voltage dependence of the "effective" Richardson constant, as it occurs in Eq. (1) for the current density of the Schottky emission.

$$F(T) \sim \ln(A^*) - \frac{q\Phi_B^0}{kT}, \tag{5}$$

and is a function only of temperature.

Thus, the representation $\ln(J/T^2)$-$V^{1/2}$ at constant temperature should be a straight line, and the intercept should be equal to $F(T)$ at the respective temperature. By looking at this representation at several temperatures and representing $F(T)$-$1/T$, it is possible to extract the potential barrier Φ_B^0 from the slope and the Richardson constant from the intercept.

An example of $\ln(J/T^2)$-$V^{1/2}$ representation is shown in Fig. 9, while $F(T)$-$1/T$ is presented in Fig. 10. The obtained values are 0.133 eV for the potential barrier at zero voltage and about 5×10^{-7} A/cm^2 K^2 for the Richardson constant. These values are remarkably similar to those obtained using the other Schottky representation, which is shown in Eq. (2). In the next section, we will try to discuss and to propose some explanations for the unusual numbers.

III. MODEL FOR THE *I-V* CHARACTERISTIC

The analysis of the experimental *I-V* characteristics, considering Eq. (1) for the current density in the case of the

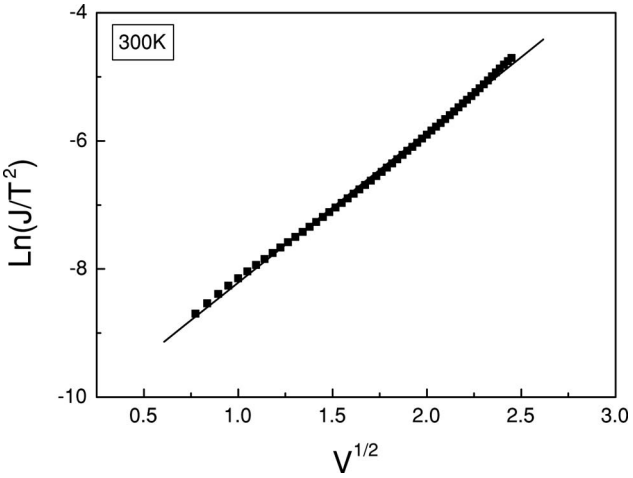

FIG. 9. Schottky representation (4) for constant temperature.

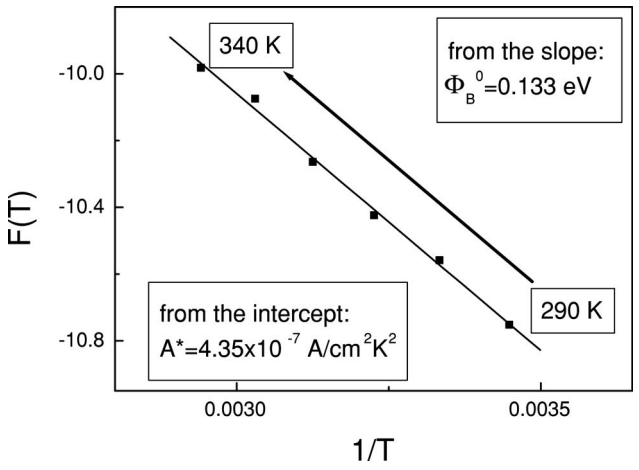

FIG. 10. Temperature dependence of the function $F(V)$ defined by Eq. (5).

Schottky emission, had revealed two important problems: (1) a lower than expected potential barrier and (2) a very low value for the effective Richardson constant. We will try to suggest some possible explanations for these unusual results.

A. The problem of the potential barrier

First, we will refer to the problem of the potential barrier, as this is related to the exponential term and has a major impact on the current magnitude. As can be seen from Eq. (1), the key quantity in the exponential term is the electric field E_m. This should be the maximum field at the Schottky barrier and, according to the newly proposed model for the metal-ferroelectric interface, its value is polarization dependent:[37]

$$E_m = \sqrt{\frac{2qN_{eff}(V + V'_{bi})}{\varepsilon_0 \varepsilon_{st}}} + \frac{P}{\varepsilon_0 \varepsilon_{st}}, \tag{6}$$

where ε_{st} is the low-frequency (or static) dielectric constant, P is the ferroelectric polarization, and N_{eff} is the effective density of fixed charge in the depletion region. That includes trapped charges and ionized shallow impurities (donors or acceptors). The electric field given by Eq. (6) is the field at the reverse-biased contact, because this is limiting the current flowing through a MFM structure. V'_{bi} is an apparent built-in potential in the presence of the polarization surface charge. Its value at the reverse-biased contact is[37]

$$V'_{bi} = V_{bi} - \frac{P}{\varepsilon_0 \varepsilon_{st}} \delta, \tag{7}$$

where V_{bi} is the normal built-in potential in the absence of ferroelectric polarization and δ is the finite distance between the surface polarization charge and the physical electrode-PZT interface. We mention that V_{bi} is the built-in potential related to the bending of the energy bands near the electrode-PZT interface. The band bending occurs due to the Fermi-level alignment through the entire MFM structure and is present irrespective of any internal bias shifting the hysteresis loop along the voltage axis. Therefore, this V_{bi} should not be associated with the internal bias producing the hysteresis imprint. As can be seen from Eq. (7), the polarization reduces the apparent built-in potential at the reverse-biased contact. For a polarization value of 100 μC/cm^2, as is the case for our films, and with a dielectric constant of 80, the reduction can be as high as 1 V for a δ value of about 1 nm.[1] The normal built-in potential is of the order of 1 V also; therefore, it can be assumed that the V'_{bi} value is very small, approaching zero, and can be neglected in Eq. (6) if $V \gg V'_{bi}$. Moreover, it will be assumed that the apparent built-in potential is negligible and that the electric field is given by

$$E_m = \sqrt{\frac{2qN_{eff}V}{\varepsilon_0 \varepsilon_{st}}} + \frac{P}{\varepsilon_0 \varepsilon_{st}}. \tag{8}$$

The first term in this equation represents the maximum electric field at a reverse-biased Schottky contact in a semiconductor material with zero polarization. The second term is due to the surface polarization charges located just near the Schottky interface. The two field components add because the polarization charges and the charges located in the depletion region of the reverse-biased contact have the same sign. Both are negative if PZT is p type, as suggested by the defect chemistry, or both are positive if PZT is n type.[1]

Placing Eq. (8) into Eq. (1) and making abstraction of the pre-exponential term, the following is obtained

$$J \sim \exp\left(-\frac{q}{kT}\left(\Phi_B^0 - \sqrt{\frac{q}{4\pi\varepsilon_0\varepsilon_{op}}\left(\frac{P}{\varepsilon_0\varepsilon_{st}} + \sqrt{\frac{2qN_{eff}V}{\varepsilon_0\varepsilon_{st}}}\right)}\right)\right). \tag{9}$$

If $\sqrt{2qN_{eff}V/\varepsilon_0\varepsilon_{st}} << P/\varepsilon_0\varepsilon_{st}$, then the current density can be written as

$$J \sim \exp\left(-\frac{q}{kT}\left[\left(\Phi_B^0 - \sqrt{\frac{qP}{4\pi\varepsilon_0^2\varepsilon_{op}\varepsilon_{st}}}\right) - \sqrt{\frac{q^2N_{eff}V}{8\pi\varepsilon_0\varepsilon_{op}P}}\right]\right). \tag{10}$$

The above equation was obtained by factorizing the polarization term in Eq. (9) and by developing the remaining radical into a series.

The exponent in Eq. (10) contains two parts. The first one includes the potential barrier at zero voltage and a polarization-dependent, voltage-independent term. The latter can be regarded as an apparent potential barrier:

$$\Phi_{B,app}^0 = \Phi_B^0 - \sqrt{\frac{qP}{4\pi\varepsilon_0^2\varepsilon_{op}\varepsilon_{st}}}. \tag{11}$$

The above equation shows that the ferroelectric polarization can significantly contribute to the apparent reduction of the potential barrier at the metal-ferroelectric interface. Thus, what was determined from the Schottky representations (2)–(5) of the experimental results is, in fact, $\Phi_{B,app}^0$ from Eq. (11). In order to get the true value of the potential barrier, as it results from the band alignment in the absence of the ferroelectric polarization, we have to estimate the second term in Eq. (11). Taking the experimental values for P and ε_{st} and considering ε_{op} of about 6.5,[38] then the potential barrier Φ_B^0 is about 0.71 eV. This value is much closer to the early

reports[11] but still might be underevaluated because of the dielectric constant. We have used the experimental value of 80, but if we use the theoretical value of about 40,[24,39] then the potential barrier is about 0.95 eV.

Regarding Eq. (11), it can be argued that for the opposite polarization orientation, the potential barrier will be increased, leading to a drastic reduction of the leakage current when the ferroelectric polarization and the applied field are antiparallel. This situation is not a steady state due to polarization switching, which can take place even at very low voltages if the dwell time is long enough.[40,41] The polarization switching adds an additional displacive contribution to current, and the measured value is no longer the true leakage current. After switching, the polarization turns parallel with the applied field and Eq. (11) holds again. Also, if the polarization is antiparallel with the applied field, then the sign of the polarization term in Eq. (6) will change because the polarization charge and the charge in the depleted region are of opposite signs. The $\sqrt{2qN_{eff}V/\varepsilon_0\varepsilon_{st}}-P/\varepsilon_0\varepsilon_{st}$ difference in Eq. (9) will turn negative if $\sqrt{2qN_{eff}V/\varepsilon_0\varepsilon_{st}}<<P/\varepsilon_0\varepsilon_{st}$. A square root from a negative quantity is not possible; therefore, either the contact turns forward bias, which is not possible because of the imposed direction of the applied field which keeps the contact reverse biased, or the polarization switches back parallel with the field.

Returning to Eq. (10), it can be seen that the second term is voltage dependent. The Schottky representation is

$$\ln(J) \sim V^{1/2}. \tag{12}$$

Thus, the $V^{1/2}$ dependence of the current density at constant temperature is still valid if the ferroelectric polarization is very high and the condition $\sqrt{2qN_{eff}V/\varepsilon_0\varepsilon_{st}}/<<P/\varepsilon_0\varepsilon_{st}$ is fulfilled. This Schottky representation is similar to that for an insulating film subject to a constant electric field. We underline that this is only an appearance induced by the presence of the surface ferroelectric charges near the reverse-biased interface.

The slope of the new Schottky representation is

$$b = \frac{q}{kT}\sqrt{\frac{q^2N_{eff}}{8\pi\varepsilon_0\varepsilon_{op}P}}. \tag{13}$$

According to Eqs. (12) and (13), from the slope of the Schottky representation, the value of N_{eff} can be estimated if P and ε_{op} are known. The value of P can be extracted from the hysteresis loops, and ε_{op} can be estimated from independent optical measurements.

B. The problem of the effective Richardson constant

The very small value for the Richardson constant shows that Eq. (1) for the current density of the Schottky emission might not be adequate. In fact, it supports Scott's suggestion that the charge injection might be interface controlled, but the transport is bulk limited, as is the case in materials with low mobility of the charge carriers.[1] In this case, the term in front of the exponential might be voltage dependent, as shown by Simmons:[42]

$$J = 2q\left(\frac{2\pi m_{eff}kT}{h^2}\right)^{3/2}\mu E\exp\left(-\frac{q}{kT}\left(\Phi_B^0-\sqrt{\frac{qE_m}{4\pi\varepsilon_0\varepsilon_{op}}}\right)\right). \tag{14}$$

The notations have the usual meanings. m_{eff} stands for the effective mass, and μ is the carrier mobility in PZT. The main problem in Eq. (14) is, again, that of the electric field. In principle, the exponential term takes the charge injection at the electrode-ferroelectric interface into consideration. This phenomenon is very sensitive to the electric field in the interface region, which is responsible for the barrier lowering by the Schottky effect. Therefore, the field E_m in the exponential term of Eq. (14) should be the maximum field at the interface.

The pre-exponential term considers the movement of the injected charges through the film volume. If the mean free path is larger than the film thickness, then the pre-exponential term is field independent and equals A^*T^2, as in Eq. (1) for thermionic emission. If the mean free path is smaller than the film thickness, then drift-diffusion processes are important and the pre-exponential term might be field dependent, as in the Simmons equation (14). The mean free path was estimated to be about 20 nm for the present epitaxial films,[32] suggesting that the Simmons equation is more appropriate. The value is larger compared to 0.1 nm estimated by Scott for polycrystalline films.[1] The difference between the two estimations might originate from different structural qualities of the films. The mean free path is certainly larger in a single-crystal-like film than in a polycrystalline, as the density of the scattering centers is very much reduced.

Equation (14) leads to the following graphic representation (we name it the Schottky-Simmons representation) at constant voltage:

$$\ln\left(\frac{J}{T^{3/2}}\right) = \ln\left(2q\left(\frac{2\pi m_{eff}k}{h^2}\right)^{3/2}\mu E\right) - \frac{q}{kT}\left(\Phi_B^0 - \sqrt{\frac{qE_m}{4\pi\varepsilon_0\varepsilon_{op}}}\right). \tag{15}$$

If the voltage is constant, then the first term in Eq. (15) is also constant, and the second term is proportional to the apparent potential barrier defined by Eq. (3). Thus, the representation $\ln(J/T^{3/2})$-$1/T$ should give a straight line. The slope will give the apparent potential barrier for the respective voltage, and the intercept will give a quantity that is proportional to μE. Figure 11 shows $\ln(J/T^{3/2})$-$1/T$ for several voltages, together with the linear fits.

The Φ_{app}-$V^{1/2}$ dependence is presented in Fig. 12, and from its intercept, a value of 0.120 eV is extracted for the potential barrier Φ_B^0. This value is similar to those obtained by using Eq. (1) for the current density, which is valid for pure thermionic emission. This result suggests that the pre-exponential term in Eq. (15) is, eventually, only very weakly dependent on the applied voltage.

We denote the pre-exponential term in Eq. (14) as $K(V)$:

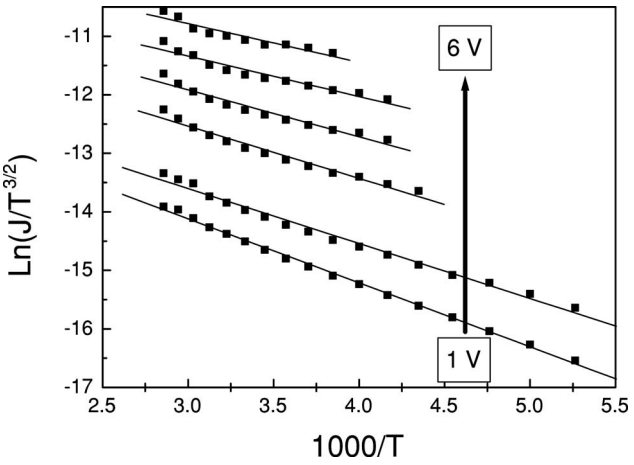

FIG. 11. Schottky-Simmons representation defined by Eq. (15).

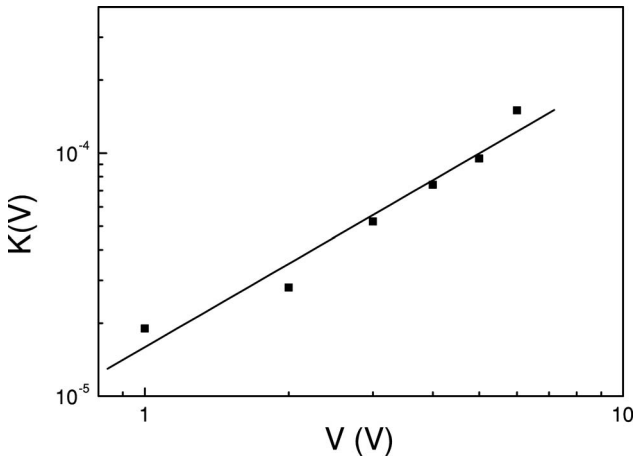

FIG. 13. Voltage dependence of the function $K(V)$ defined by Eq. (16).

$$K(V) = 2q\left(\frac{2\pi m_{eff}k}{h^2}\right)^{3/2}\mu E(V). \tag{16}$$

It was assumed that this term might be voltage dependent through the μE product. The $K(V)$ values for different voltages were determined from the intercepts of the Schottky-Simmons representations shown in Fig. 11. They are presented in Fig. 13 as function of the applied voltage. The representation was done in log-log scale and the linear fit gives a slope of about 1.1, suggesting a linear dependence of the $K(V)$ term on the applied voltage V. Furthermore, this fact suggests that the product μE should be proportional to the applied voltage. If the mobility is assumed field independent, then the result is that the electric field E is proportional to V and not to $V^{1/2}$, as is the field E_m given by Eq. (8).

It can be imagined that the injected carriers are subjected to the E_m field at the interface, but in the bulk, they experience a smaller field E. From the theory of the Schottky contact, it is known that the electric field in the depleted region is strongly dependent on position. Thus, it can be assumed that the electric field decreases from some maximum value E_m at the interface to some constant value E in the bulk. Both quantities are voltage dependent, but with different laws. Although it was derived from different premises, the idea of a nonuniform electric field inside a ferroelectric film was suggested earlier by Dawber and Scott[43] in the model developed to explain a negative differential resistance and a positive temperature coefficient observed in some polycrystalline $(Ba,Sr)TiO_3$ films. Although negative differential resistance and positive temperature coefficient features were not observed in our epitaxial PZT samples, a nonuniform electric field might exist according to Zubko *et al.*[44] The thermodynamic model developed for films with space charges found that the electric field inside the film can be nonuniform. Referring to this model, we did not experimentally observe, at any thickness, the predicted significant reduction of polarization due to space charges. This could be due to the fact that the model assumes static space charges, neglecting the fact that the hysteresis measurement is a dynamic one and that the charged defects have a time response which is dependent on the depth of the associated energy level in the forbidden band.[45]

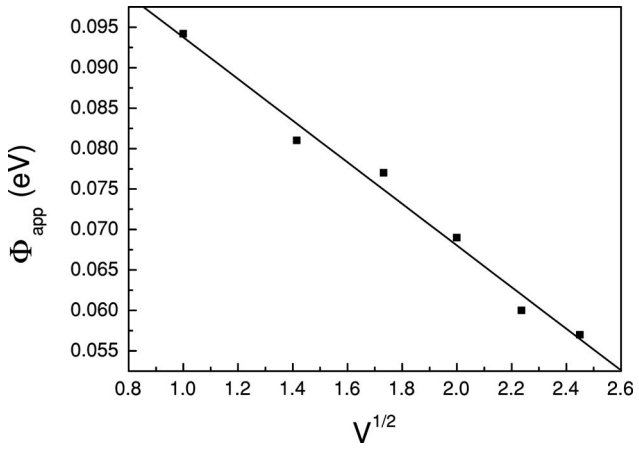

FIG. 12. Voltage dependence of the apparent potential barrier deduced from the Schottky-Simmons representations at several constant voltages. The intercept gives the potential barrier at 0 V which is about 120 meV.

Moreover, from the slope of the $K(V)$-V representation, it should be possible to estimate the mobility μ [see Eq. (16)] and if we assume that the field E is the ratio between the voltage V and the film thickness d. That will require the knowledge of the effective mass m_{eff}

The latter can be estimated from the FN representation at low temperatures. In the FN formalism, the current density is given by

$$J \sim E^2 \exp\left[-\frac{4\sqrt{2m_{eff}}(q\Phi_B^0)^{3/2}}{3q\hbar E}\right]. \tag{17}$$

Assuming that at low temperatures (below 70 K) the film is fully depleted because the carriers are frozen on the energy levels in the gap, the representation $\ln(J/V^2)$-$1/V$ should be a straight line. The slope is

$$b_{\mathrm{FN}} = \frac{4\sqrt{2m_{eff}}(q\Phi_B^0)^{3/2}d}{3q\hbar}. \tag{18}$$

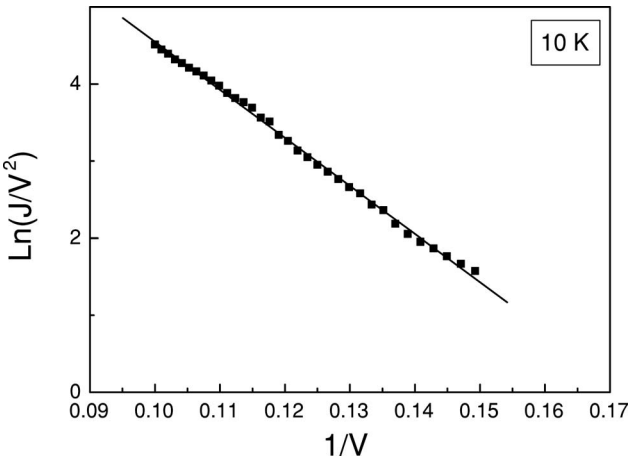

FIG. 14. FN representation at 10 K. The slope is used to evaluate the effective mass.

An example of FN representation is shown in Fig. 14 for a temperature of 10 K. Referring to Eqs. (17) and (18), we mention that the potential barrier Φ_B^0 should be taken as the apparent potential barrier $\Phi_{B,app}^0$, which includes the effect of the ferroelectric polarization on the interface properties. Hysteresis measurements have shown that the polarization has only a weak temperature dependence being practically constant down to 4.2 K. Also, capacitance-voltage measurements performed at low temperatures have shown that the capacitance of the investigated film becomes relatively constant for voltages above 6–7 V, suggesting full depletion. The capacitance in these ranges of temperature and field is about 290 pF, which results in a dielectric constant of about 72. Since both the polarization and dielectric constant are not very much different from the values around room temperature, we have assumed that the apparent potential barrier also depends only weakly on temperature. Therefore, taking the potential barrier as 0.12 eV and the film thickness of 215 nm, we have obtained a value of $0.8m_0$ for the effective mass. m_0 is the mass of the free electron. This value for the effective mass is between the values of $4.3m_0$ extracted from the simulations of the *I-V* characteristics[21] and $0.09m_0$ extracted from *C-V* measurements.[4] This value should be regarded as a rough estimate, as the voltage interval for the FN plot is not very large. Above 10 V, the ferroelectric capacitor suffers from irreversible breakdown, while below 7 V, the FN representation does not fit the experimental data. We suppose that at low fields, although the temperature is low, the conduction mechanism is a mixture of Schottky-Simmons and Fowler-Nordheim.

The value of $0.8m_0$ was then used to estimate a value of about 10^{-6} cm^2/V s for the mobility from the slope of the $K(V)$-V representation (see Fig. 14). This value is also a rough estimate, as the error can be up to 2 orders of magnitude, depending on the value used for the effective mass. Also, it does not include a temperature dependence of the mobility and is dependent on the assumption that the field E is given by V/d. The last hypothesis is very approximate, as the product μE might have a linear dependence on V without having a d^{-1} dependence on thickness. In any case, it appears that the estimated value of mobility is small compared with other reports, presenting numbers in the 1–1400 cm^2/V s range,[46–49] but it is larger than the mobility of the oxygen vacancies.[50–52]

Recently, it was shown that the mobility can be considerably reduced in highly polar semiconductor alloys. A model was developed for AlGaN, and it was found that the mobility can be reduced from about 3000 cm^2/V s to less than 10 cm^2/V s.[53] This is a reduction of almost 3 orders of magnitude in a material with polarization of a few μC/cm^2. It can be assumed that in PZT, which has a much higher polarization, the reduction of the mobility for the injected carriers is even higher.

A change in the mobility should be reflected by a change in the electric conductivity, and thus in the conductance of the film. We have imagined an experiment to check if there is a direct link between the conductance and the polarization. We took a virgin contact and performed hysteresis measurements by gradually increasing the amplitude of the 1 kHz triangular voltage. After each hysteresis measurement, we have performed a conductance-frequency (*G-f*) measurement with the aid of a HP4194A impedance and/or gain analyzer. The results of the hysteresis and *G-f* measurements are shown in Fig. 15.

The results show that, as the hysteresis loop opens and the ferroelectric polarization increases toward saturation, the conductance of the film at low frequencies decreases. Thus, as the polar order increases, the dc conductance decreases, supporting the idea that the mobility of the injected carriers is very much reduced when the polar order increases and the film goes to a monodomain state.

We have performed some simulations for temperatures of 200, 250, 300, and 350 K using the Schottky-Simmons equation (14). The following values were used: effective mass of $0.8m_0$, an average static dielectric constant of 80, an optic dielectric constant of 6.5, a polarization of 1 C/m^2, and an apparent potential barrier of 0.12 eV. The simulated curves are shown in the inset of Fig. 4, together with the experimental data. The mobility had to be adjusted from 10^{-7} cm^2/V s at 200 K to about 3×10^{-6} cm^2/V s at 350 K, but the average value over the selected temperature range is about 10^{-6} cm^2/V s. As expected, the voltage range where the simulated curves fit the experimental ones is wider at higher temperatures. This suggests that at lower temperatures and higher voltages, the FN tunneling through the tip of the potential barrier becomes significant, overlapping with the Schottky-Simmons mechanism. The results of the simulations are in agreement with Fig. 11, also showing that the Schottky-Simmons plot at higher voltages is adequate on a smaller range of temperatures. At the end of this section, it can be concluded that the ferroelectric polarization appears to influence not only the potential barrier at the electrode-ferroelectric interface but also the mobility of the injected carriers.

Here, we point out that the possible d^{-1} thickness dependence of the pre-exponential term in Eq. (14), as suggested above, will be difficult to be experimentally observed. Accurate thickness dependence can be extracted from Eq. (14) only if the exponential term, which is thickness independent, is the same for films with different thicknesses. Unfortunately, the exponential term might be sample dependent.

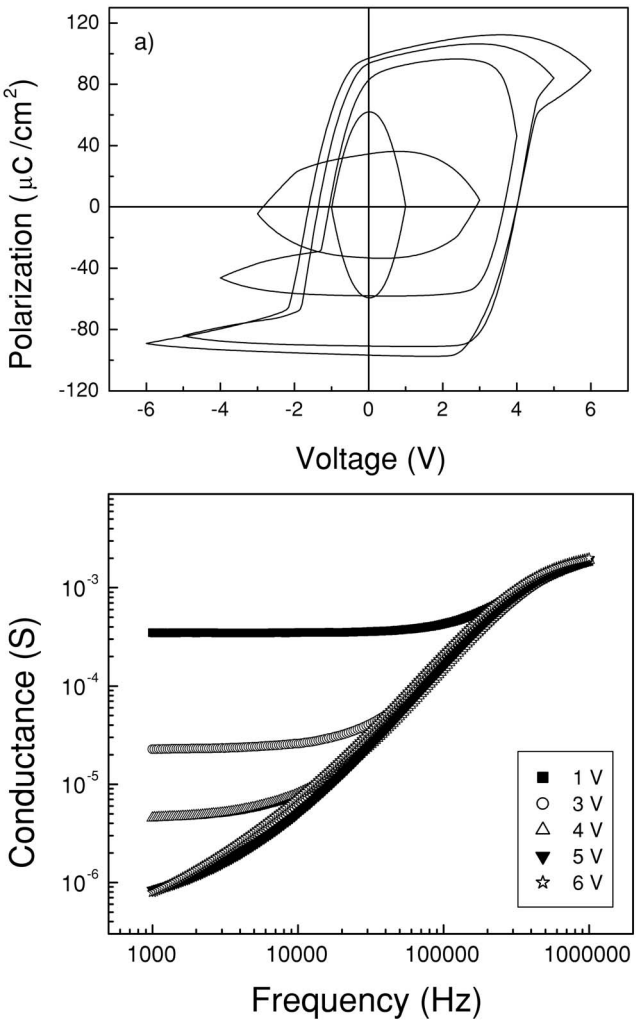

FIG. 15. (a) Hysteresis loops and (b) *G-f* characteristics for several amplitudes of the triangular voltage applied to a virgin contact. First, the hysteresis loop was measured at a certain amplitude, and then the *G-f* characteristic was recorded without any dc voltage and with a 100 mV ac voltage.

There are several reasons for which the exponential term can vary and the most important might be the following:

(1) The potential barrier at the metal-PZT might slightly vary from sample to sample. The potential barrier is very sensitive to interfacial states.[1] Present deposition methods do not allow accurate control of the density of the interface states. A minute variation in the density of the interface states can affect the potential barrier with a few meV, sufficient to hide the expected thickness dependence.

(2) The total density of the point defects N_{eff}, entering in the exponential term through the maximum field at the interface E_m, might be sample dependent. A small variation in the density of the point defects, such as impurities or vacancies, will change the exponential term from sample to sample, making it difficult to extract any thickness dependence from the pre-exponential term.

(3) Polarization value might be slightly different from film to film. In our case, the measured values are about 100 μC/cm^2, with a variation of ± 7 μC/cm^2. This will also impact the exponential term, which is directly dependent on polarization, making it again difficult to extract the thickness dependence of the pre-exponential factor.

A variation of 10 in the film thickness should reflect in a variation of 10 of the current density given by Eq. (14) if the exponential term is the same for different thicknesses. This variation can be hidden by a variation of only 50 meV of the apparent potential barrier given by Eq. (3). A variation of this magnitude can be produced by a change of 10% in polarization (e.g., from 95 to 105 μC/cm^2) or a variation of up to 1 order of magnitude in N_{eff} (e.g., $10^{19}-10^{20}$ cm^{-3}).

C. Defects and leakage current

Returning to Eq. (8), it can be seen that the electric field in the interface region is very much dependent on the effective density of fixed charges in the depleted region. N_{eff} does not only include the ionized shallow impurities, either donors or acceptors, but also the charged traps. Any structural defect in the PZT film might act as a trapping center for the charge carriers. Point defects, dislocations, and even domain walls (especially the 90° domains) can trap carriers. In the energy diagram, the trapping centers are represented as energetic levels in the forbidden band of PZT. At equilibrium, all the traps above the Fermi level are empty from electrons and all the traps below the Fermi level are filled with electrons. A voltage applied to the MFM structure will disrupt the equilibrium by changing the band bending in the interface regions and by injecting charge carriers from the electrodes. Some of the injected carriers might be trapped in the interface regions, if the applied voltage drives empty trapping levels below the quasi-Fermi level. When the perturbation is removed, these carriers will be released. Thus, there will be an emission time constant from the trap, which sets the time-frequency response of the trapping center. In the case of dc measurements, the delay time used for the *I-V* characteristics was long enough to prevent transient currents from the traps. The emission time constant of the traps is strongly dependent on temperature according to the following equation:[45]

$$\tau_n = \left[\sigma_n \upsilon_{th,n} N_C \exp\left(-\frac{E_C - E_T}{kT} \right) \right]^{-1}. \tag{19}$$

Here, σ is the capture cross section, υ_{th} is the thermal velocity, N_C is the density of states in the conduction band, and E_T is the depth of the trap level below the conduction band E_C. The subscript n is for electron traps, but a similar equation stands for the hole traps.

Equation (19) tells us that a trap level is filled at low temperatures when the emission time constant goes to infinity and is empty at high temperature when τ goes to zero. It results that the quantity N_{eff} is dependent on temperature. N_{eff} is defined by[45,54]

$$N_{eff}(T) = \sum_i n_{h,i}(T) - \sum_j n_{n,j}(T) + N_{dop}, \tag{20}$$

where $n_{h,j}$ is the density of the jth trap level for holes, $n_{n,i}$ is the density of the ith trap level for electrons, and N_{dop} is the

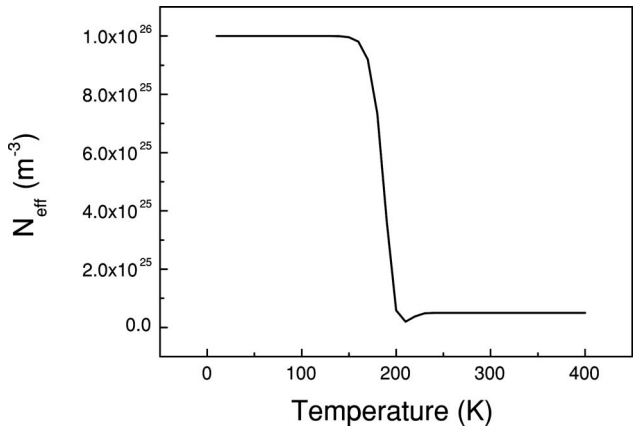

FIG. 16. Simulated temperature dependence for the fixed charge density N_{eff} in the depleted region. The simulation was performed by assuming one trapping level for electrons and one for holes, with different depths in the forbidden band and different concentrations.

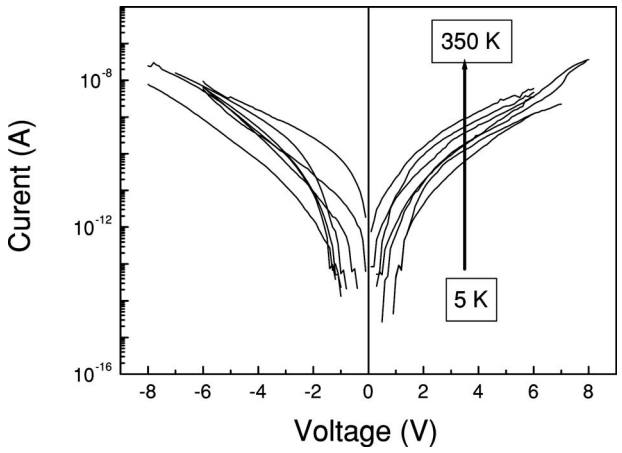

FIG. 17. Temperature behavior of the *I-V* characteristic in the case of a defective sample. The unknown temperature dependence of N_{eff} leads to an unpredictable temperature behavior of the *I-V* characteristic. No valuable information can be extracted in this case.

doping density. It can be seen that, depending on the densities of the electron and holes traps and depending on their energetic depth in the forbidden band, N_{eff} can change not only the value but also the sign during a temperature measurement; that will have a large influence on the value E_m of the electric field at the interface and on the density of the injected current [see Eqs. (8)–(10) and (14)]. Figure 16 shows how the density N_{eff} can vary with temperature for a situation with one electron and one hole trapping levels and a doping concentration of about 10^{18} cm^{-3}.[1] Usual numbers were used for the traps parameters. It is not the purpose of this paper to explain in detail the possible trapping levels in PZT. The only purpose of Fig. 16 is to show that N_{eff} can be different at different temperatures, and that these changes in N_{eff} lead to a complicated temperature dependence of the *I-V* characteristics in more defective samples. It can happen that, on such samples, the current density does not follow a clear temperature dependence for a constant voltage. The Schottky representation (2) makes no sense in such cases, and no valuable information can be extracted following the above presented analysis.

An example of such a sample is given in Fig. 17. As can be seen, the *I-V* characteristics at different temperatures cross each other, with no clear trend with increasing temperature. For a given voltage, the current value does not vary as expected in the temperature range from 5 to 350 K. This behavior shows how important the temperature dependence of N_{eff} can be. It is possible that, on small temperature regions, one or the other conduction mechanism proposed for PZT films fits the experimental data. However, our belief is that such results are not conclusive as long as the microstructure effects are neglected. The extrapolation of such models to larger temperature regions or to samples with different microstructures and compositions is not appropriate.

Finally, using relation (13), we have evaluated N_{eff} at room temperature for several samples with different thicknesses. The obtained values are in the 10^{19}–10^{20} cm^{-3} range. It was observed that the samples with higher density of fixed charges show, in general, a smaller polarization. The difference was up to 10 μC/cm^2 only. This fact agrees with the suggestion that charged defects pin the ferroelectric domains, leading to a smaller polarization. We underline that our films possess a negligible density of extended defects, namely, dislocations or 90° domain walls; thus, most of the traps contributing to N_{eff} are probably point defects.

Further studies are needed in order to clarify the problem of deep traps in PZT films. Undoubtedly point defects exist, such as oxygen (V_O) and lead vacancies (V_{Pb}), but the characteristics of the associated trap levels are not well known.[55] The point defects can form complexes with other atoms from the lattice. There are theoretical studies supporting the formation of a V_O-Ti^{3+} complex, which is an effective electron trap.[56–58] Other point defects can also be present, inducing deep trap levels in the forbidden band.[59–61]

D. Other potential candidates for the conduction mechanism near room temperature

If at temperatures below 100 K the only possible candidate for the conduction mechanism is the Fowler-Nordheim tunneling, at temperatures in the 250–350 K range, the situation is not so clear. The above presented results might be explained by the bulk-controlled Schottky injection in the sense that the charge injection from the electrodes is controlled by the interface properties but the drift from the injecting electrode to the collecting one is dominated by the slow mobility in the bulk. The emerging picture is that of a strongly nonuniform electric field in the film, with very large values at the interfaces and with a smaller but constant value in the bulk of the film. This picture resembles the Matterhorn model proposed by Scott.[1]

However, following the general assumption that the ferroelectric films are mainly insulating, with constant electric field inside, other conduction mechanisms could also be considered. The first one is the simple thermal activation of some conduction channel, for example, by exciting the carriers to some trapping level at the electrode-PZT interface followed by the tunneling into the valance band of the ferro-

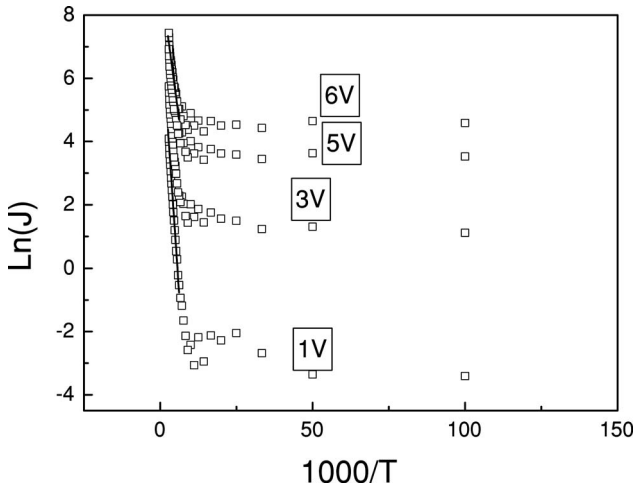

FIG. 18. Arrhenius plots ln J-1/T for several voltages applied to the MFM structure.

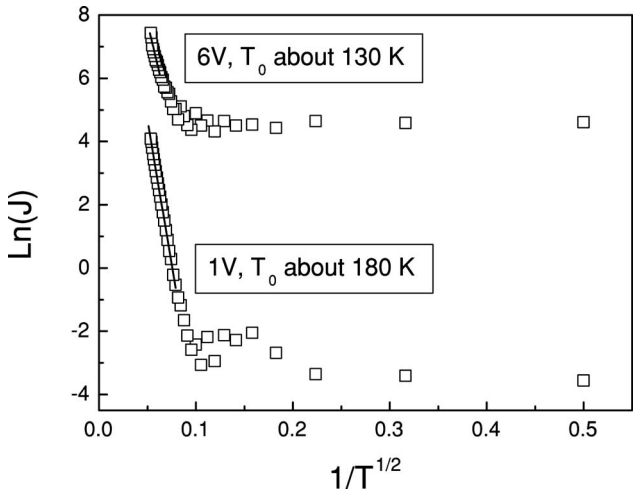

FIG. 20. ln J-1/$T^{1/2}$ representation in the case of 1D hopping.

electric (assumed to be p type). This is the so-called trap-assisted tunneling.[62–65] The simple Arrhenius representation ln J-1/T, shown in Fig. 18, will give an activation energy E_A, which is the difference between the trap level energy in the PZT and the common Fermi level in the MFM structure. We have represented the Arrhenius plot for several voltages, and from the slopes, we have extracted the activation energy E_A. The values should be the same, as both the Fermi level and the trapping level bend with the same quantity qV when an external voltage is applied, but it is not the case, as we observed that E_A has a $V^{1/2}$ dependence (see Fig. 19). Therefore, we can assume that this conduction mechanism is not adequate to describe the charge transport around room temperature.

Finally, another possibility would be the unidimensional hopping, which has the following temperature dependence:[66]

$$J \sim \exp\left[-\left(\frac{T_0}{T}\right)^{1/2}\right]. \tag{21}$$

T_0 is a characteristic temperature related to the onset of the hopping mechanism. The representation ln J-1/$T^{1/2}$ is shown in Fig. 20 for the two extreme voltages of 1 and 6 V. The linear fit is very good at the low voltage and for temperatures above 130 K, giving a T_0 value of 180 K. For the high voltage, the linear fit is not as good and gives a T_0 value of about 150 K. It can be assumed that the carrier injection is somehow controlled by the interfaces and might depend on the voltage. Once injected into the ferroelectric film, the carriers will experience a constant field, which will drive them to the opposite electrode. Thus, the carrier hopping from one defect to the other is not random but is mostly along the direction of the external field.

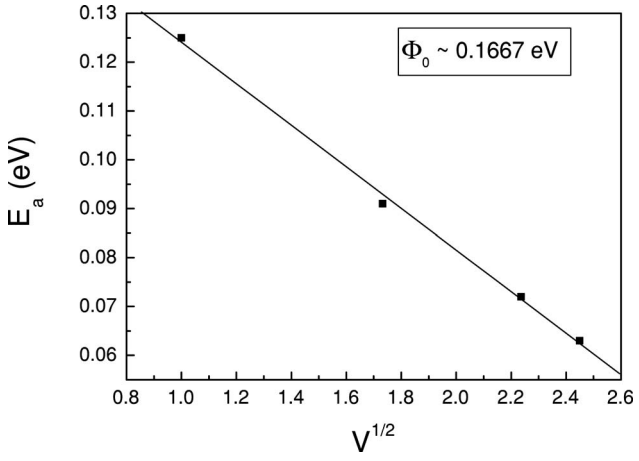

FIG. 19. Voltage dependence of the activation energy E_A extracted from the Arrhenius plots.

The questions are how the hopping takes place and which defects are involved. In GaN films, such unidirectional (one-dimensional) hopping is usually associated with the presence of threading dislocations,[65] and the hopping taking place along the dislocation path, but this picture does not fit for the studied tetragonal PZT films in which threading dislocations are absent. Only some point defects can be involved in this case, and these can be the oxygen vacancies V_O. It was theoretically shown that V_O have the tendency to order along the polarization axis,[56] making the 1D hopping possible. However, the question is whether the concentration V_O is high enough to enable the hopping. The agreed concentration is in the 10^{20} cm^{-3} range; thus, there will be a vacancy at about every five unit cells along the polarization direction. This will lead to a hopping distance of about 2 nm, which is not unphysical considering that the critical hopping distance in Si nanowires was found to be about 8–9 nm.[66] Therefore, the unidirectional variable range hopping might be a candidate for the dominant conduction mechanism above about 150 K, but this must be verified by further experiments and theoretical models. A theory for the I-V characteristic of the hopping mechanism in ferroelectrics is not yet available.

IV. CONCLUSIONS

The voltage dependence of the leakage current was studied in epitaxial PZT films with thicknesses in the 50–350 nm range. It was found that the magnitude of the leakage current

density and the shape of the *I-V* characteristic are only weakly dependent on the film thickness. This fact, coupled with the marked asymmetry of the positive and negative branches of the *I-V* characteristics, suggests the dominance of interface-controlled mechanisms.

An analysis of the *I-V* characteristics measured at different temperatures was performed by assuming the dominance of the Fowler-Nordheim tunneling at low temperatures and of the Schottky emission at high temperatures. Some unexpected results were obtained, such as very low values for the potential barrier and for the pre-exponential factor in the formula of the current density of the Schottky emission. These were explained by assuming a direct effect of the ferroelectric polarization on the potential barrier value and on the carrier mobility. The experimental results point toward a model in which the charge injection is interface controlled, but the movement of the charge carriers from one electrode to the other is bulk limited. This might be due to a large reduction of carrier mobility as a consequence of the dipolar order. The results also hint toward a nonuniform electric field inside the PZT film, with very large values at the injecting interface and with a lower but nonzero value in the bulk.

It was also shown that the structural defects acting as trapping centers for the charge carriers, and contributing to the density of fixed charge N_{eff} in the depleted region, can strongly affect the temperature behavior of the *I-V* characteristic.

Other candidates for the dominant conduction mechanism near room temperature might be the trap-assisted tunneling and the 1D hopping.

ACKNOWLEDGMENTS

This work was supported by the Volkswagen Stiftung under Contract No. I/77738. Some of the theoretical work was made in collaboration with the DINAFER-2-CEEX-06-11-44 project.

[1] J. F. Scott, in *Ferroelectric Memories*, Advanced Microelectronics Series, edited by K. Itoh and T. Sakurai (Springer-Verlag, Berlin, 2000).
[2] I. Stolichnov and A. Tagantsev, J. Appl. Phys. **84**, 3216 (1998).
[3] B. Nagaraj, S. Aggarwal, T. K. Song, T. Sawhney, and R. Ramesh, Phys. Rev. B **59**, 16022 (1999).
[4] J. C. Shin, C. S. Hwang, H. J. Kim, and S. O. Park, Appl. Phys. Lett. **75**, 3411 (1999).
[5] S. Horii, S. Yokoyama, H. Nakajima, and S. Horita, Jpn. J. Appl. Phys., Part 1 **38**, 5378 (1999).
[6] D. P. Chu, Z. G. Zhang, P. Migliorato, B. M. McGregor, K. Ohashi, K. Hasegawa, and T. Shimoda, Appl. Phys. Lett. **81**, 5204 (2002).
[7] J. D. Baniecki, T. Shioga, K. Kurihara, and N. Kamehara, J. Appl. Phys. **94**, 6741 (2003).
[8] B. Chen, H. Yang, L. Zhao, J. Miao, B. Xu, X. G. Qiu, B. R. Zhao, X. Y. Qi, and X. F. Duan, Appl. Phys. Lett. **84**, 583 (2004).
[9] T. P. Juan, S. Chen, and J. Y. Lee, J. Appl. Phys. **95**, 3120 (2004).
[10] Y. S. Yang, S. J. Lee, S. H. Kim, B. G. Chae, and M. S. Jang, J. Appl. Phys. **84**, 5005 (1998).
[11] I. Stolichnov, A. Tagantsev, N. Setter, J. S. Cross, and M. Tsukuda, Appl. Phys. Lett. **75**, 1790 (1999).
[12] B. Nagaraj, S. Aggarwal, and R. Ramesh, J. Appl. Phys. **90**, 375 (2001).
[13] S. Aggarwal and R. Ramesh, Annu. Rev. Mater. Sci. **28**, 463 (1998).
[14] M. E. Lines and A. M. Glass, *Principles and Applications of Ferroelectrics and Related Materials* (Clarendon, Oxford, 1977).
[15] M. W. Chu, I. Szafraniak, R. Scholz, C. Harnagea, D. Hesse, M. Alexe, and U. Goesele, Nat. Mater. **3**, 87 (2004).
[16] V. Nagarajan, A. Roytburd, A. Stanishevsky, S. Prasertchoung, T. Zhao, L. Chen, J. Melngailis, O. Auciello, and R. Ramesh, Nat. Mater. **2**, 43 (2003).
[17] C. L. Canedy, Hao Li, S. P. Alpay, L. Salamanca-Riba, A. L. Roytburd, and R. Ramesh, Appl. Phys. Lett. **77**, 1695 (2000).
[18] S. P. Alpay, I. B. Misirlioglu, V. Nagarajan, and R. Ramesh, Appl. Phys. Lett. **85**, 2044 (2004).
[19] I. Vrejoiu, G. Le Rhun, L. Pintilie, D. Hesse, M. Alexe, and U. Goesele, Adv. Mater. (Weinheim, Ger.) **18**, 1657 (2006).
[20] I. Vrejoiu, G. Le Rhun, N. D. Zakharov, D. Hesse, L. Pintilie, and M. Alexe, Philos. Mag. **86**, 4477 (2006).
[21] L. Pintilie and M. Alexe, J. Appl. Phys. **98**, 124103 (2005); L. Pintilie, I. Boerasu, M. J. M. Gomes, T. Zhao, R. Ramesh, and M. Alexe, *ibid.* **98**, 124104 (2005).
[22] M. J. Haun, E. Furman, S. J. Jang, and L. E. Cross, Ferroelectrics **99**, 63 (1989).
[23] D. Vanderbilt and R. D. King-Smith, Phys. Rev. B **48**, 4442 (1993).
[24] S. Tinte, K. M. Rabe, and D. Vanderbilt, Phys. Rev. B **68**, 144105 (2003).
[25] N. Sai, K. M. Rabe, and D. Vanderbilt, Phys. Rev. B **66**, 104108 (2002).
[26] H. Morioka, S. Yokoyama, T. Oikawa, K. Saito, and H. Funakubo, Appl. Phys. Lett. **85**, 3516 (2004).
[27] H. Morioka, G. Asano, T. Oikawa, K. Saito, and H. Funakubo, Appl. Phys. Lett. **82**, 4761 (2003).
[28] T. Oikawa, M. Aratani, H. Funakubo, K. Saito, and M. Mizuhira, J. Appl. Phys. **95**, 3111 (2004).
[29] K. R. Udayakumar, P. J. Schuele, J. Chen, S. B. Krupanidhi, and L. E. Cross, J. Appl. Phys. **77**, 3981 (1995).
[30] H. Fujisawa, S. Nakashima, K. Kaibara, M. Shimizu, and H. Niu, Jpn. J. Appl. Phys., Part 1 **38**, 5392 (1999).
[31] S. H. Kim, H. J. Woo, J. Ha, C. S. Hwang, H. R. Kim, and A. I. Kingon, Appl. Phys. Lett. **78**, 2885 (2001).
[32] L. Pintilie, I. Vrejoiu, D. Hesse, G. LeRhun, and M. Alexe, Phys. Rev. B (to be published).
[33] S. M. Sze, *Physics of Semiconductor Devices*, 2nd ed. (Wiley, New York, 1981), Chaps. 7 and 10.
[34] J. Frenkel, Phys. Rev. **54**, 647 (1938).
[35] I. Stolichnov and A. Tagantsev, J. Appl. Phys. **84**, 3216 (1998).

[36] M. Dawber, K. Rabe, and J. F. Scott, Rev. Mod. Phys. **77**, 1083 (2005).
[37] L. Pintilie and M. Alexe, J. Appl. Phys. **98**, 124103 (2005).
[38] I. Boerasu, L. Pintilie, M. Pereira, M. I. Vasilevskiy, and M. J. M. Gomes, J. Appl. Phys. **93**, 4776 (2003).
[39] P. Ghosesz (private communication).
[40] A. Gruverman, B. J. Rodriguez, C. Dehoff, J. D. Waldrep, A. I. Kingon, R. J. Nemanich, and J. S. Cross, Appl. Phys. Lett. **87**, 082902 (2005).
[41] Y. W. So, D. J. Kim, T. W. Noh, Jong-Gul Yoon, and T. K. Song, Appl. Phys. Lett. **86**, 092905 (2005).
[42] J. G. Simmons, Phys. Rev. Lett. **15**, 967 (1965).
[43] M. Dawber and J. F. Scott, J. Phys.: Condens. Matter **16**, L515 (2004).
[44] P. Zubko, D. J. Jung, and J. F. Scott, J. Appl. Phys. **100**, 114112 (2006).
[45] D. K. Schroeder, *Semiconductor Material and Device Characterization* (Wiley-Interscience, New York, 1998).
[46] H. H. Wang, F. Chen, S. Y. Dai, T. Zhao, H. B. Lu, D. F. Cui, Y. L. Zhou, Z. H. Chen, and G. Z. Yang, Appl. Phys. Lett. **78**, 1676 (2001).
[47] D. Nagano, H. Funakubo, K. Shinozaki, and N. Mizutani, Appl. Phys. Lett. **72**, 2017 (1998).
[48] Y. S. Yang, S. J. Lee, S. H. Kim, B. G. Chae, and M. S. Jiang, Jpn. J. Appl. Phys., Part 1 **36**, 749 (1997).
[49] D. C. Lupascu, Phys. Rev. B **70**, 184124 (2004).
[50] S. Zafar, R. E. Jones, B. Jiang, B. White, V. Kaushik, and S. Gillespie, Appl. Phys. Lett. **73**, 3533 (1998).
[51] M. Dawber and J. F. Scott, Appl. Phys. Lett. **76**, 1060 (2000).
[52] A. Q. Jiang, J. F. Scott, M. Dawber, and C. Wang, J. Appl. Phys. **92**, 6756 (2002).
[53] W. Zhao and D. Jena, J. Appl. Phys. **96**, 2095 (2004).
[54] P. Braeunlich, *Thermally Stimulated Relaxation in Solids* (Springer, Berlin, 1979).
[55] R. Waser and D. M. Smyth, in *Ferroelectric Thin Films: Synthesis and Basic Properties*, edited by C. Paz de Arauji, J. F. Scott, and G. W. Taylor, Ferroelectricity and Related Phenomena Series Vol. 10 (Princeton Resources, Princeton, 1996), p. 47.
[56] C. H. Park and D. J. Chadi, Phys. Rev. B **57**, R13961 (1998).
[57] K. T. Li and V. C. Lo, J. Appl. Phys. **97**, 034107 (2005).
[58] S. Poykko and D. J. Chadi, Phys. Rev. Lett. **83**, 1231 (1999).
[59] J. Robertson, J. Appl. Phys. **93**, 1054 (2003).
[60] J. Robertson, Appl. Phys. Lett. **63**, 1519 (1993).
[61] V. V. Laguta, M. D. Glinchuk, I. P. Bykov, Yu. L. Maksimenko, J. Rosa, and L. Jastrabik, Phys. Rev. B **54**, 12353 (1996).
[62] P. C. Arnette and D. J. DiMaria, J. Appl. Phys. **47**, 2092 (1976).
[63] O. Blank, H. Reisinger, R. Stengl, M. Gutsche, F. Wiest, V. Capodieci, J. Schulze, and I. Eisele, J. Appl. Phys. **97**, 044107 (2005).
[64] D. Mahaveer Sathaiya and Shreepad Karmalkar, J. Appl. Phys. **99**, 093701 (2006).
[65] E. J. Miller, E. T. Yu, P. Waltereit, and J. S. Speck, Appl. Phys. Lett. **84**, 535 (2004).
[66] H. Iwano, S. Zaima, and Y. Yasuda, J. Vac. Sci. Technol. B **16**, 2551 (1998).